Cross-Talk between Receptor Tyrosine Kinases AXL and ERBB3 Regulates Invadopodia Formation in Melanoma Cells

Cross-talk between receptor tyrosine kinases AXL and ERBB3 regulates invadopodia formation in melanoma cells

Or-Yam Revach[1], Oded Sandler[1], Yardena Samuels[1] and Benjamin Geiger[1]*

[1] Department of Molecular Cell Biology, Weizmann Institute of Science, Rehovot 7610001, Israel

List of Abbreviations

RTK- Receptor Tyrosine Kinase

MMPs- Metalloproteinases

ECM- Extracellular Matrix

KD- Knock-down

DK- Dead-Kinase

SFK- Src Family Kinases

***Corresponding author:**

B. Geiger

Tel: +972-8-934-3910

Mobile: +972-52-348-8848

Email: benny.geiger@weizmann.ac.il

The authors declare no potential conflicts of interest.

Abstract

The invasive phenotype of metastatic cancer cells is accompanied by the formation of actin-rich invadopodia, which adhere to the extracellular matrix and degrade it. In this study, we explored the role of the tyrosine kinome in the formation of invadopodia in metastatic melanoma cells. Using a microscopy-based siRNA screen, we identified a series of regulators, the knock down of which either suppresses (e.g., TYK2, IGFR1, ERBB3, TYRO3, FES, ALK, PTK7) or enhances (e.g., ABL2, AXL, CSK) invadopodia formation and function. Notably, the receptor tyrosine kinase AXL displayed a dual regulatory function, where both depletion or overexpression enhanced invadopodia formation and activity. This apparent contradiction was attributed to the capacity of AXL to directly stimulate invadopodia, yet its suppression upregulates the ERBB3 signaling pathway, which can also activate core invadopodia regulators and enhance invadopodia function. Bioinformatic analysis of multiple melanoma cell lines points to an inverse expression pattern of AXL and ERBB3. High expression of AXL in melanoma cells is associated with high expression of invadopodia components and an invasive phenotype. These results provide new insights into the complexity of metastasis-promoting mechanisms and suggest that targeting of multiple invadopodia signaling networks may serve as a potential anti-invasion therapy in melanoma.

Introduction

The morbidity and mortality rates caused by melanoma tumors are primarily associated with the high capacity of these tumors to metastasize, resulting in a 10-year survival rate of 12.5-26% (1). The initial steps of the metastatic process include local invasion of the melanoma cells into the surrounding connective tissue, driven by signaling pathways that stimulate cell migration across

tissue barriers; turnover of cell-matrix and cell-cell adhesions; and penetration of the cancerous cells into the vascular and lymphatic systems (2). The migratory and invasive processes are commonly driven by reorganization of the actin cytoskeleton, and the formation of protrusive cell structures such as lamellipodia, filopodia, ruffles, and invadopodia (3).

Invadopodia are actin-rich protrusions of the plasma membrane, which attach to the extracellular matrix (ECM) via integrin receptors, and degrade it (4). These structures are commonly found in metastatic cancer cells, and are believed to promote the dissemination of metastases *in vivo* (5). The local invasion-promoting activity of invadopodia is achieved by coordination of local adhesions, enzymatic degradation of the ECM, and the development of physical protrusive force, generated by actin polymerization, that pushes the plasma membrane outward (4,6). Their proteolytic activity, exerted by secreted and membrane-bound metalloproteinases (MMPs), and serine proteinases (7) distinguishes invadopodia from other migration-promoting membrane protrusions (e.g., lamellipodia, filopodia) or ECM adhesions (e.g., focal adhesions, podosomes) (5).

The temporal sequence of events that drives invadopodia formation and function is not fully understood; yet it has been proposed that this process is initiated by ligand-induced activation of receptor tyrosine kinases (RTKs) (8) that activate Src family kinases (9), and the PI3K-AKT pathway (10). Consequently, TKS5 (5,11), and cortactin (12) are phosphorylated, and participate in the early stages of actin machinery assembly in invadopodia (5,6). A few RTKs, such as members of the EGFR family (13) , the DDR family kinases (14), and Tie2 (15), were shown to affect invadopodia formation and function, suggesting that tyrosine phosphorylation is a major regulator of invadopodia formation and function in different cells. That said, an understanding of

the specific roles of individual kinases in the regulation of invadopodia formation and action remains limited.

We addressed the issue in this study by conducting a microscopy-based siRNA screen, targeting each of the 85 human tyrosine kinases in A375 metastatic melanoma cells, and tested the effect of their knock-down (KD) on invadopodia formation and on ECM degradation. The screen revealed 7 kinases (TYK2, IGFR1, ERBB3, TYRO3, FES, ALK, PTK7), whose suppression decreased invadopodia function, and 3 kinases (ABL2, AXL, CSK) whose KD increased invadopodia function. Testing the involvement of these genes in the regulation of invadopodia formation in another metastatic melanoma cell line, 63T, confirmed some, but not all, of the regulators identified in the original screen, which may be attributed to a different driver mutation in the cells (a BRAF/NRAS mutation in A375/63T cells, respectively) and cell-specific variations in the tyrosine kinome.

In-depth characterization of the role of the AXL RTK in invadopodia formation indicated that this kinase exerts a dual role as an invadopodia regulator, with an intrinsic capacity to stimulate invadopodia; yet its suppression up-regulates an alternative signaling pathway for invadopodia formation: the ERBB3 signaling pathway, which can activate core invadopodia regulators, and greatly enhance invadopodia formation and function. We discuss the mechanism underlying the apparent cross-talk between AXL and ERBB3, and its potential relevance to metastatic melanoma therapy.

Materials and Methods

Antibodies and reagents

R428 inhibitor and Gas6 were purchased from R&D Systems (Minneapolis, MN, USA). R428 was used at concentrations of 1-5 μM, depending on the cell type. Gas6 was used at a range of concentrations, 200ng-1,000 ng/ml, depending on the cell type. Effective concentrations of Gas6 varied between experiments. Neuregulin was purchased from PeproTech (Rocky Hill, NJ, USA) and was used in concentrations of 100 ng/ml. Puromycin was used for selection of infected cells at concentrations of 3μg/ml (Sigma St. Louis, MO, USA).

Antibodies used in this study included: Mouse monoclonal anti-phosphorylated tyrosine is a self-prepared soup Rabbit polyclonal anti p-AXL(Y779) was purchased from R&D Systems. Rabbit monoclonal antibody anti p-ERBB3 (Y1289) # 4791; rabbit polyclonal antibody anti-Cortactin # 3503; and rabbit polyclonal antibody p-SRC (Y416) # 2101 were ordered from Cell Signaling (Danvers, MA, USA). Mouse monoclonal anti-ERBB3, SC-7390; rabbit polyclonal anti-TKS5; goat polyclonal anti-AXL, SC-1096; rabbit polyclonal anti-SRC, SC-19; rabbit polyclonal anti-AKT, SC-8312 and rabbit polyclonal anti-p-AKT (s437), SC-514032 were supplied by Santa Cruz Biotechnology (Dallas, TX, USA). Mouse monoclonal anti-GAPDH, #AM4300, came from Thermo Fisher Scientific (Waltham, MA, USA). F-Actin was fluorescently labeled with TRITC-phalloidin from Sigma-Aldrich (St. Louis, MO, USA). Nuclei were labeled with DAPI staining (Sigma).

Secondary antibodies used in this study included: Goat anti-mouse IgG conjugated to Cy5 (Jackson ImmunoResearch Laboratories, West Grove, PA, USA); goat anti-rabbit IgG H&L

(HRP) #ab97080; and goat anti-mouse IgG H&L (HRP) #ab97040 (Abcam, Cambridge Science Park, Cambridge, UK).

Plasmids, siRNA and transfections

IRES-GFP empty vector, AXL-WT-IRES-GFP, and AXL-KD-IRES GFP were a kind gift from Dr. Aaron S. Meyer (Koch Institute for Integrative Cancer Research at MIT, Cambridge, MA, USA).

DNA transfection: Cells were transfected using Lipofectamine2000 (Invitrogen, Carlsbad, CA, USA) in antibiotic-free media, according to the manufacturer's instructions. Media were replaced with full media after 6 h. After 48 h, cells were replated onto cross-linked gelatin-coated plates (see Gelatin coating section, below) for 3-6 h, depending on the experiment, then either fixed, or lysed for protein.

RNA transfection: Transfection of the siRNA siGENOME SMARTpool™ (GE Healthcare Dharmacon, Lafayette, CO, USA) was performed using DharmaFect1 (Dharmacon) at a 50 μM concentration. In every transfection, siNON-TARGETING POOL #2 was used as a control, with siTOX as the transfection efficiency reporter. Cells were incubated for 48 h before replating for an experiment. RNA sequences are listed in Supplementary Material 1.

AXL knock-down by shRNA: TRC AXL shRNA was purchased from GE Healthcare Dharmacon. pCMV-VSV-G (helper plasmid) and pHRCMV-8.2ΔR (packaging plasmid) were both kindly provided by Prof. Yardena Samuels (Weizmann Institute of Science, Rehovot, Israel). Mission pLKO.1-puro (Sigma-Aldrich) was used as a negative control vector. HEK293 cells were transfected with the target plasmid, together with the helper and the packaging plasmid, using Lipofectamine 2000 (Invitrogen). Conditioned medium was collected from the

cells 48h post-transfection, and placed on the target cells (A375) for 24 h. Cells were treated with 3μg/ml puromycin for selection.

Cell cultures

A375 metastatic melanoma cells, HEK293T, 4T1 and MDA-231 metastatic breast carcinoma cells were obtained from the American Type Culture Collection (ATCC) (Manassas, VA, USA). WM793 and A2508 cells were a kind gift from Prof. Meenhard Herlyn (Wistar Institute, Philadelphia, PA, USA). All human cell lines, except 293T cells, were authenticated using STR profiling in the last year.

A subset of cell lines (104T, 63T and 76T) used in the study were derived from a panel of pathology-confirmed metastatic melanoma tumor resections collected from patients who consented by written approval to enroll to an immunotherapy study. The trails were approved by the Institutional Review Board and conducted by the US Common Rule. Clinical trials (#03-C-0277) were conducted at the Surgery Branch of the National Cancer Institute (Bethesda, MD, USA). Pathology-confirmed melanoma cell lines were derived from mechanically or enzymatically dispersed tumor cells. All patient derived cell lines were authenticated using STR profiling. Cells were cultured in DMEM or RPMI medium supplemented with 10% FCS (Gibco, Grand Island, NY, USA), 2 mM glutamine, and 100 U/mL penicillin-streptomycin. Cultures were maintained in a humidified atmosphere of 5% CO_2 in air, at 37°C. Mycoplasma tests were carried out routinely using a mycoplasma PCR detection kit (BI CT, USA) or by mycoplasma fast kit (Biotool, TX, USA). Last check for A375 cells was on September 27, 2018.

Quantitative real-time PCR (QRT–PCR)

Total RNA was isolated using an RNeasy Mini Kit (Qiagen, Valencia, CA, USA), according to the manufacturer's protocol. A 2 μg aliquot of total RNA was reverse-transcribed, using a high-capacity cDNA reverse transcription kit (Applied Biosystems, Carlsbad, CA, USA). Quantitative real-time PCR (QRT–PCR) was performed with an OneStep instrument (Applied Biosystems), using Fast SYBR® Green Master Mix (Applied Biosystems). Gene values were normalized to a GAPDH housekeeping gene. Primer sequences can be found in Supplementary Material 1.

Gelatin coating

Gelatin gel: 96-well glass-bottomed plates (Nunc, Thermo Fisher Scientific) or plastic tissue culture plates were coated with 50 μg/ml poly-L-lysine solution (Sigma, catalogue # P-7405) in Dulbecco's PBS, and incubated for 20 min at room temperature. The plates were then gently washed 3 times with PBS. Porcine skin gelatin, 0.2 mg (Sigma, catalogue #G2500) was dissolved at 37°C in 100 ml ddH_2O. Gelatin was cross-linked with 1-ethyl-3-(3-dimethylaminopropyl) carbodiimide (EDC, Sigma, catalogue #03450) and N-hydroxysuccinimide (NHS, Sigma, catalogue #130672), each prepared as 10% solutions in ddH_2O. The 96-well glass-bottomed plates were coated with 50 μl of gelatin and cross-linker mixture, and the plastic plates were coated with various volumes, according to their size. The ratios of gelatin to cross-linkers were 82.5:12.5:5 (gelatin: NHS: EDC).

Surfaces were incubated for 1 h at room temperature, washed 3 times in PBS, and sterilized by 30 min of UV radiation.

Immunofluorescence staining, immunofluorescence microscopy, and image analysis

For immunostaining, cells were plated at ~70% confluence on gelatin-coated glass-bottomed plates (see above) for varying time periods. Cells were then fixed for 3 min in warm 3% PFA (Merck, Darmstadt, Germany), 0.5% Triton X-100 (Fluka-Chemie AG, Switzerland), followed by 3% PFA alone for an additional 30 min. Post-fixation, cells were washed 3 times with PBS and incubated with primary antibody for 1 h, washed 3 times in PBS, and incubated for an additional 30 min with the secondary antibody, washed again, and kept in PBS for imaging. Images were acquired using the DeltaVision microtiter system (Applied Precision, Inc., Issaquah, WA, USA), using a 40x/0.75 air objective, or a 60x/1.42 oil objective (Olympus, Tokyo, Japan). Image analysis was performed using ImageJ software (rsbweb.nih.gov/ij).

Gelatin degradation assay

Fluorescently labeled gelatin (0.2 mg porcine skin gelatin; Sigma, catalogue #G2500) was prepared by Alexa Fluor™ 488 (A10235)/ Alexa Fluor™ 546 Protein Labeling Kit), molecular probes, Thermo Fisher Scientific, according to the manufacturer's instructions. Glass-bottomed 96-well plates were coated as mentioned above (gelatin coating), with ratios of 1:10 labeled gelatin: non-labeled gelatin.

For degradation assays, cells were plated on the gelatin matrix, and cultured for varying lengths of time (on average, 5-6 h). Cells were fixed and stained for actin and DAPI, and degradation area was assessed by ImageJ software.

In every well, 36-64 fields of view were imaged in an automated fashion by the DeltaVision microtiter system, using a 40x objective. Cells in every field of view were counted using DAPI

staining, and the degradation area was calculated by the fluorescently labeled gelatin channel, using the Analyze Particles plug-in in ImageJ software. The value for each well assessing invadopodia function was total degradation area/cell (μm^2). To compare results between experiments, control values were normalized to 1, and all the samples were normalized accordingly.

For R428 inhibitor experiments, cells were plated on gelatin-coated plates with the indicated concentrations of the inhibitor (1-5 μM, depending on the cell type) or DMSO, and fixed after 5 h. For prolonged R428 treatment, cells were cultured with the indicated concentrations of the inhibitor (1-2 μM, depending on the cell type) or DMSO for 2 days, then replated on gelatin-coated plates with the same inhibitor concentrations, and fixed (after 5 h) for the invadopodia assay.

For Gas6 stimulation, A375 cells were cultured with 200-1000 ng/ml of Gas6 for 5 h. Cells were fixed and stained for actin and DAPI, invadopodia function was assessed as mentioned above, and the results compared to control cells. For 63T cells, Gas6 stimulation in concentrations of 100-1000 ng/ml was conducted under 1% serum conditions (only throughout the duration of the experiment).

Immunoblotting

Whole-cell lysates were prepared using SDS lysis buffer (2.5% SDS, 25% glycerol, 125 mM Tris-HCL pH=6.8, 0.01% bromophenol blue, and 4% freshly added beta-mercaptoethanol). Samples were resolved on 8% SDS-PAGE gels, and transferred into PVDF/nitrocellulose membranes. Blots were probed with antibodies to AXL (1:1000), p-ERBB3 (1:1000), ERBB3 (1:500), pCortactin (1:1000), cortactin (1:1000), pSRC (1:1000), Src (1:1000), pAKT (1:1000),

AKT (1:1000), and GAPDH (1:1000) (see Antibodies and reagents section, above), and developed using SuperSignal® ECL reagents (Thermo Fisher Scientific).

For R428 inhibitor experiments, cells were plated on gelatin-coated plates with the indicated concentrations of the inhibitor (1-2 μM, depending on the cell type) or DMSO, and lysed for immunoblotting after 3 h. For prolonged R428 treatment, cells were cultured with the indicated concentrations of the inhibitor (1-2 μM, depending on the cell type) or DMSO for 2 days, then replated on gelatin-coated plates with the same inhibitor concentrations, and lysed for immunoblotting after 3 h.

Cell invasion assay

A375 cells (50,000 cells) were cultured in serum-free media in the upper chamber of a BioCoat Matrigel Invasion Chamber #354480 (Corning, NY, USA), in duplicates. Full medium containing 10% FBS was placed in the lower chamber. Cells were allowed to invade into the Matrigel for 24 h, then fixed with methanol, and stained with Gimsa. Cells that remained in the upper part of the chamber were removed with a cotton bud, and the inserts were washed 3 times, before imaging the inserts. Four quarters were imaged for each filter using a 10x lens, and cells were counted manually, using an ImageJ cell counter. Cell counts from the two duplicates were averaged. Each experiment was normalized to its control, as a percentage of invading cells.

Screen targeting tyrosine kinome using siRNA

A screen for invadopodia regulators among tyrosine kinase family members was performed, using a tyrosine kinase library (siGENOME SMARTpool™, Dharmacon) for A375 and 63T metastatic melanoma cells (see Cell cultures section for details of cell lines).

The siRNA library targets 85 genes of the tyrosine kinome (See Supplementary Material 2). Cells were cultured in a 96-well plate format in antibiotic-free media, 1 day prior to transfection. The next day, the siRNA library was transfected into the cells, using a DharmaFect1 protocol calibrated to achieve the highest transfection efficiency in those cells. Cells were transfected with 50 μM siRNA that targets tyrosine kinases, using non-targeting siRNA as a control (Supplementary Fig. 1A). In each experiment, siTOX was used to test transfection efficiency in a qualitative fashion.

In order to test transfection efficiency in a quantitative fashion, a few wells in every experiment were transfected with siCON (non-targeting control) or with siSRC, and Src levels were analyzed using real-time PCR. Transfection efficiency was 80-90%. The following day, the medium was replaced by full media, and cells were incubated for another 48 h. Three days following transfection, cells were replated in fluorescently labeled gelatin on 96-well glass-bottomed plates (see Gelatin coating section, above). After 6 h, cells were fixed and stained for actin, TKS5 and DAPI. Plates were then imaged in an automated fashion with a DeltaVision microtiter system, using a 40x objective. In each well, 16-36 fields of the gelatin, actin, TKS5 and DAPI were imaged automatically by the microscope; each field was then analyzed using ImageJ software for degradation/cell (μm^2), and all the fields were quantified into average degradation rates per cell (Supplementary Fig. 1A).

Quantities and shapes of invadopodia were analyzed in a quantitative and qualitative fashion, using actin and TKS5 staining (Table 1, Phenotype; Supplementary Material 2; and Supplementary Fig. 1B, 1C).

In Supplementary Material 2, data from the 3 screens in the A375 cell line, and from the 2 screens in the 63T cell line, are presented. In every tab, control values are presented first,

followed by all the genes that were analyzed. Degradation values were normalized to control, that was set as 1, in order to compare different experiments. A *p*-value was calculated for each gene, according to the degradation/cell values in all the fields, relative to the control values. In the first screen, only KD of genes that showed any effect on matrix degradation (52 of 85 tyrosine kinases) were analyzed. Genes whose KD caused a statistically significant difference (*p* value ≤ 0.05) and led to a $\leq$ 3-fold reduction or a $\geq$ 1.5-fold elevation or more in gelatin degradation, were chosen for further validation (Supplementary Material 2, Screen 2). Altogether, the primary screen was performed three times (See results in Supplementary Material 2).

In 63T cells, the 10 invadopodia regulators which were found in A375 cells were tested two additional times (Supplementary Material 2).

Invadopodia quantification

Invadopodia quantification was determined as a percentage of invadopodia-forming cells in 16-36 fields, based on their actin and TKS5 labeling. Cell counts were performed by DAPI, as described above.

Gene expression analysis

Gene expression profiles of AXL, ERBB3, MITF, and three of the MITF targets (PMEL, TYRP1, and MELANA), were extracted from 62 melanoma cell lines from the *CCLE* dataset (https://portals.broadinstitute.org/ccle) containing Affymetrix microarray expression data. Hierarchical clustering by Euclidian distance was applied on the Z-score values, and four groups of cell lines were manually defined. *P*-values were calculated for the differences between

ERBB3 and AXL levels, and the other 4 genes within each group (see Supplementary Material 3, tab 1). Invadopodia-related genes and tyrosine kinases were compared only between two groups of cell lines with alternating patterns of AXL and ERBB3 (Clusters 1 and 2) (see 23, tabs 2 and 3). Significance level was determined by a Mann-Whitney two-tailed test, following multiple hypothesis correction.

Human Phosphotyrosine-RTK Array

A Human Phosphotyrosine-RTK array (R&D Systems, Wiesbaden-Nordenstadt, Germany, No. ARY001) was performed, according to the manufacturer's instructions. Briefly, cells were lysed on ice in lysis buffer with protease inhibitors (Sigma) for 15 minutes. Five hundred micrograms of lysates were incubated with blocked array membranes overnight. Detection was performed using an enhanced Chemiluminescent SuperSignal West Femto substrate (Thermo Fisher Scientific, Rockford, IL, USA).

Statistical analysis

Quantitative data for statistical analysis were expressed as mean ± SEM (shown as an error bar) from at least three independent experiments, unless stated otherwise. The significance of the difference between samples was calculated using a two-tailed Student's t-test. *P*-value > 0.05 - n.s (not significant); *p*-value ≤ 0.05 *; *p*-value ≤ 0.01 **; *p*-value ≤ 0.001 ***; *p*-value ≤ 0.0001 ****.

Results

Primary screen for novel invadopodia regulators in melanoma cells

The search for invadopodia regulators was conducted by siRNA screening, whereby each of the human tyrosine kinases was knocked down from the metastatic human melanoma cell line A375 (See Supplementary Material 2). These cells form prominent invadopodia in 30-40% of the cells (16), displaying a moderate capacity to degrade the underlying gelatin matrix, and enabling the quantification of both suppression and enhancement of matrix degradation. Immunolabeling of these cells for phosphotyrosine, together with actin, as a marker for invadopodia, revealed extensive localization of tyrosine-phosphorylated residues both within invadopodia cores, and throughout the adhesion rings surrounding them (Fig. 1A; invadopodia are denoted by white arrows). A comparable level of labeling was also detected in focal adhesions located mainly at the cell periphery (Fig. 1A).

The siRNA 'SMARTpool' library was transfected into A375 cells in a 96-well format, and transfection efficiency was found to be 80-90%, based on the ability of siTOX to kill the cells (Fig. 1B), or quantitative real-time PCR analysis of Src in Src KD cells (Fig. 1C). To assess the effect of tyrosine kinase KD on invadopodia function, the treated cells were replated on fluorescently labeled gelatin in 96-well glass-bottomed plates for 6 h, then fixed and stained for actin and TKS5, as invadopodia markers, and DAPI, for cell number quantification and assessment of cell toxicity (Supplementary Fig. 1A). Plates were then imaged automatically (see Materials and Methods), and gelatin degradation area/ per cell (μm^2) was quantified (Supplementary Fig. 1A and Supplementary Material 2). To compare the results of the different experiments, gelatin degradation values were normalized to the control, which was set as 1.

Invadopodia formation was evaluated qualitatively, based on staining for actin and TKS5 (Table1, Phenotype). For the final list of regulators, quantitative analysis of the percentage of invadopodia-forming cells was performed (Supplementary Fig. 1B, 1C). Only genes whose KD resulted in a statistically significant difference (p value < 0.05) and led to a >3-fold reduction or a >1.5-fold elevation in gelatin degradation, compared to control, were selected for further characterization (Supplementary Material 2, Screen 2). Altogether, the primary screen was performed three times (See full results in Supplementary Material 2).

Of the 85 human tyrosine kinases tested, KD of 7 genes reproducibly reduced gelatin degradation, while 3 enhanced it (Table 1; Fig. 1D-1F). Notably, all the genes KD that affected gelatin degradation also induced comparable changes in invadopodia formation (Table 1, Phenotype; and Supplementary Fig. 1B, 1C). KD of each of the three genes causing an elevation in invadopodia function (CSK, AXL and ABL2) resulted in an increase in the percentage of cells forming invadopodia with a high content of TKS5 in their cores (Table 1, Phenotype; Supplementary Fig. 1B, 1C). In contrast, KD of most genes that caused reduction in gelatin degradation resulted in a decrease in invadopodia-forming cells (Table 1, Phenotype; Supplementary Fig. 1B, 1C).

Notably, some of the invadopodia-regulating genes identified in this screen were previously shown to affect invadopodia formation or function, including CSK (17), which inhibits the activity of Src family kinases (18) and, upon KD, causes a dramatic elevation in invadopodia function. PTK7 and ERBB3 were shown to be positive invadopodia regulators in other cellular systems (19,20), and ABL2 was found in our screen of melanoma cell lines to be a negative regulator, while in breast cancer cells, it was shown to positively regulate invadopodia (13,21).

Given the potential functional redundancy between tyrosine kinases, which may vary in different cell types, we further tested the effectiveness of the regulators that were found in A375 on another metastatic, patient-derived melanoma cell line, 63T, which differs from A375 cells in its genetic background (a BRAF/NRAS mutant in A375/63T cells, respectively (22). 63T cells displayed conspicuous invadopodia with extensive matrix degradation in 20-30% of the cells, (Fig. 2A), and are suitable for siRNA transfection (Fig. 2B, 2C). Testing the effects of siRNA KD of the A375 invadopodia regulators on 63T cells (see Supplementary Material 2) indicated that only KD of FES, one of the 7 positive regulators obtained with A375 cells, also induced a reduction in invadopodia function in 63T cells. Conversely, the 3 regulators whose KD enhanced invadopodia in A375 cells (CSK, AXL and ABL2), displayed a similar effect in 63T cells (Supplementary Table 1; Fig. 2D; and Supplementary Fig. 1D).

AXL is a receptor tyrosine kinase, associated with an invasive phenotype in multiple cancers, including melanoma (23,24). In addition, AXL was shown to be involved in drug resistance mechanisms in melanoma and other cancers (25).

Intrigued by the unexpected enhancement of invadopodia following the KD of AXL, and its novel association with invadopodia regulation, we chose to focus our study on the mechanism underlying the effect of this kinase on invadopodia formation and function.

The AXL RTK regulates invadopodia in melanoma cells

To validate the specificity of the augmentation of invadopodia prominence and matrix degradation upon AXL KD, we tested each of the four duplexes present in the siRNA 'SMARTpool' in both A375 and 63T cell lines, and confirmed that 3 out of 4 siRNA duplexes

display an elevated degradation effect similar to that seen in the siAXL siRNA pool (Supplementary Fig. 2A, 2B). Further quantification of the effect indicated that upon KD of AXL, normalized gelatin degradation levels (degraded area/cell) increased by a factor of 7 (in A375 cells) or of 4 (63T cells) (Fig. 3A-C). AXL suppression efficiency was up to 90%, as determined by Western blot (Fig. 3D) and real-time PCR (Supplementary Fig. 2C, 2D). Percentage of invadopodia-forming cells in both cell lines was elevated comparably to the increased gelatin degradation (Fig. 3E, 3F, respectively). A similar effect involving elevated invadopodia function was obtained when cells were stably infected with shAXL (Supplementary Fig. 2E, 2F), and upon siRNA transfection in two other melanoma cell lines, WM793 and A2508, that also form invadopodia (Supplementary Fig. 2G-I).

The role of invadopodia in elevated matrix degradation induced by AXL suppression was confirmed by double KD of both AXL and TKS5 (an invadopodia-specific marker), which eliminated the elevation in matrix degradation (Supplementary Fig. 2J, 2K).

Finally, localization of phosphorylated AXL in A375 and 63T melanoma cells, as seen by immunofluorescence microscopy, pointed to a strong association of AXL with invadopodia cores at various time points following cell culturing and invadopodia formation (Fig. 3G, 3H). Taken together, these results suggest that AXL plays an important role in the regulation of invadopodia in melanoma cells.

AXL is a dual-function regulator of invadopodia, with both suppressive and stimulatory activity

Further characterization of the molecular mechanisms underlying the role of AXL in invadopodia formation and function indicated that AXL might have a dual regulatory effect, both negative and positive. First, we tested the effect of AXL overexpression on invadopodia function

(e.g., gelatin degradation) in A375 cells (Fig. 4A, 4B) or in 63T cells (Fig. 4C). The over-expression of wild-type AXL, but not of its kinase-dead (DK) derivative, or empty vector, caused a significant elevation in invadopodia function, suggesting that kinase activity is required for the positive regulation of invadopodia (Fig. 4A-C). The transfection resulted in a marked elevation in total AXL levels (Supplementary Fig. 3A). The elevation in gelatin degradation also correlated with the ability of the cells to invade through a transwell filter *in vitro* (Supplementary Fig. 3B, 3C). The localization of both the WT and DK mutant of AXL to the membrane was confirmed by immunolabeling of non-permeabilized 293T cells (that do not express endogenous AXL), following transfection with the WT and mutant AXL, compared to an empty vector (Supplementary Fig. 3D).

Additional support for the positive role of AXL in invadopodia formation and function in A375 or 63T melanoma cells was obtained through elevated levels of invadopodia, following treatment with the AXL ligand Gas6 (26) (Fig. 4D, 4E and Supplementary Fig. 3E), that did not cause elevation in AXL KD cells (Supplementary Fig. 3F). In addition, there was suppression of invadopodia in both cell types by treatment with the AXL inhibitor R428 for 6h [Fig. 4F, 4G (A375) and 4H, 4I (63T)]. Invadopodia inhibition by the AXL inhibitor was also observed in two additional, patient-derived melanoma cells lines, 76T and 104T, as well as in 4T1 murine metastatic breast cancer cells that form invadopodia (Supplementary Fig. 3G, 3H). Elevated levels of invadopodia function upon AXL KD was specific to melanoma cells, as when AXL was KD in MDA-231 breast cancer cells, invadopodia function was decreased by factor of two (Supplementary Fig. 3I, 3J), corroborating our observation that AXL acts as a general positive invadopodia regulator.

ERRB3 activation is up-regulated upon AXL suppression, leading to enhanced invadopodia function

Given existing evidence that AXL promotes invasion and migration in a variety of cancer cells (23,24), together with our current findings, we hypothesized that an alternative invasion-promoting pathway may be activated following AXL inhibition by siRNA, leading to an elevation in invadopodia formation. Furthermore, this alternative pathway is not activated following short-term inhibition of AXL by R428 (Fig. 4F-I).

Surprisingly, the levels of pAXL (phosphorylated on Y779) were not decreased, and even slightly elevated, in AXL KD cells, compared to control (Fig. 5A; quantifications in 5B), although total AXL levels were decreased by about 90% (Fig. 5A). However, RTK array, total phosphotyrosine analysis, revealed a ~50% reduction in AXL phosphorylation on other tyrosine residues (Supplementary Fig. 4A, 4B). Further staining of AXL KD cells showed strong localization of pAXL (Y779), in invadopodia (Supplementary Fig. 4C). Moreover, short-term inhibition (up to 6h) of AXL KD cells by R428, caused a reduction of AXL phosphorylation on Y779, demonstrated by Western blot (Fig. 5A, 5B) and cell staining (Supplementary Fig. 4C). Reduced invadopodia function was detected following this treatment (Supplementary Fig. 4D). These results indicate that the residual AXL (10-15%) in AXL KD cells is hyper-phosphorylated on Y779 and strongly localized to invadopodia structures, suggesting that this phosphorylation may be important for invadopodia function. These findings led us to hypothesize that another tyrosine kinase is driving AXL hyper-phosphorylation, thereby enhancing invadopodia formation.

Cross-talk between AXL and EGFR family members was previously proposed by studies in several cancer systems as a potential mechanism for drug resistance, usually in the form of AXL activation following EGFR inhibition (27–29). Moreover, in breast cancer cells, the opposite process was found, when prolonged inhibition of AXL leads to an increase in ERBB3 expression and phosphorylation (30). This phenotype was not linked to invasion or invadopodia. Moreover, to our knowledge, no such interplay between AXL and ERBB3 was documented in melanoma cells.

When we analyzed, in A375 cells, the levels of ERBB3 activation under conditions of AXL KD, we found an increase in total ERBB3 levels, as well as in ERBB3 phosphorylation (Fig. 5C). RNA levels of ERBB3 were only slightly elevated following AXL inhibition (Supplementary Fig. 4E), suggesting that the up-regulation of ERBB3 is primarily post-transcriptional. It is noteworthy that the interplay between AXL and ERBB3 was not symmetrical, as ERBB3 KD did not affect AXL levels and phosphorylation on Y779 (Supplementary Fig. 4F; quantifications in Supplementary Fig. 4G). In line with that, Gas6 stimulation did not rescue invadopodia function in ERBB3 KD cells (Supplementary Fig. 4H). Moreover, Src, Cortactin and AKT activating phosphorylation levels were also elevated under those same conditions (Fig. 5D, 5E, and 5F, respectively, quantifications to all western blots shown in Fig. 5G). Activation of these components is an indication of more active invadopodia, and higher levels of actin polymerization (4). Indeed, the SRC and PI3K-AKT pathways can potentially be activated directly by ERBB3 (31), and cortactin is a downstream target of Src in invadopodia formation (5). These results suggest that AXL inhibition activates the ERBB3 pathway in melanoma cells, and this activation may lead to an increase in invadopodia formation.

Consistently, invadopodia function was also elevated following long term (2 days) inhibition of AXL by the R428 inhibitor, comparable to that observed following AXL siRNA-mediated KD (Fig. 5H), and in contrast with short-term (6h) exposure to the inhibitor, which blocks invadopodia formation (Fig. 4F-4I). Moreover, prolonged AXL inhibition using R428 results in higher levels of total and phosphorylated ERBB3 (Fig. 5I, 2 right lanes). Notably, no such elevation was observed following short-term (6h) treatment with the inhibitor (Fig. 5I, 2 left lanes). Cortactin phosphorylation was also elevated under prolonged AXL inhibition using R428 (Fig. 5J, 2 right lanes), and not under short-term treatment (Fig. 5J, two left lanes). Quantifications of ERBB3 and cortactin upon inhibitor treatment are shown in Fig. 5K.

The notion that the elevation in invadopodia function in AXL KD cells depends on ERBB3 activation was further tested by double-KD experiments. In accordance with the siRNA screen, KD of ERBB3 alone led to suppression of invadopodia activity, while AXL KD increased it (Fig. 5L and 5M). Double KD of AXL and ERBB3 indicated that invadopodia elevation by AXL KD does not take place in the absence of ERBB3 (Fig. 5L and 5M). Specifically, the difference between invadopodia function following ERBB3 KD and AXL+ERBB3 double KD was found to be highly significant (Fig. 5L and 5M).

Finally, Neuregulin, an ERBB3 ligand (32), stimulation elevated invadopodia function in both A375 and 63T cells (Fig. 5N, 5O), and resulted in slightly higher invadopodia activity in AXL KD cells, compared to non-treated AXL KD cells (Supplementary Fig.4I).

To further test if AXL KD affects other RTKs, we analyzed the phosphorylation of all 49 RTKs, using an RTK array (Supplementary Fig. 4A, 4B). As shown, ALK and ERBB3 phosphorylations were slightly elevated, while VEGFR2 and AXL phosphorylations were

reduced upon AXL KD (Supplementary Fig. 4A, 4B). No further alterations in the phosphorylation of RTKs were detected upon AXL KD.

Our findings suggest that when AXL is suppressed or inhibited for prolonged periods, the ERBB3 pathway, an alternative, highly potent signaling pathway for invadopodia formation, is activated, leading to increased invadopodia formation and function. This increase in invadopodia function can be directly mediated by ERBB3 or indirectly, through over-activation of AXL by phosphorylation on tyrosine 779 (Fig. 5A). (See further activation mechanism in the Discussion below).

AXL expression exhibits an expression pattern inverse to that of ERBB3 and MITF in melanoma cells

To test whether the interplay between AXL and ERBB3 constitutes a common feature of melanoma cells, we analyzed the expression levels of AXL and ERBB3 in 62 melanoma cell lines from the *CCLE* database (https://portals.broadinstitute.org/ccle). MITF and three of its downstream targets were added to the analysis, due to the known inverse correlation of AXL and MITF expression levels in melanoma, and the relevance of the MITF/AXL ratio to melanoma state, progression and drug resistance (33).

On the CCLE database-derived expression Z-score values, we applied hierarchical clustering, and four groups of cell lines were manually defined (Figure 6A). Two of the clusters (Cluster 1 and Cluster 2; a total of 31 cell lines) encompassing 50% of the dataset, displayed a distinct, inverse expression pattern between AXL and ERBB3 (p-value <0.0006; see Supplementary Material 3). Moreover, ERBB3 expression levels were positively correlated with the levels of MITF and its downstream targets (Fig. 6A, Clusters 1 and 2). Clusters 3 and 4 showed different

expression patterns: either all three genes (AXL, ERBB3 and MITF) were expressed at high levels (Fig. 6A, cluster 3); or both ERBB3 and AXL were highly expressed, but MITF was low (Fig. 6A, Cluster 4). This analysis demonstrates that in many cases of melanoma (50%, in our dataset), the expression patterns of AXL and ERBB3 are mutually exclusive, suggesting that they act on alternative oncogenic pathways, as we see in the context of invadopodia regulation (Fig. 5).

Next, we classified the cells as proliferative or invasive, based on their melanoma phenotype-specific expression (MPSE) signature (34,35). MPSE predicts whether the cell phenotype will be proliferative or invasive, based on the expression of a set of genes. Cluster 1 (AXL low/ERBB3 high) is enriched with proliferative cell lines (Fig. 6B, lower bar), whereas Cluster 2 (AXL high/ERRB3 low) is dominated by an invasive phenotype (Fig. 6B, lower bar).

Consistently, Cluster 2 exhibits a significantly higher expression of invadopodia components [e.g., TKS5 (SH3PXD2A), Fascin, MMP2, ABL1, and vinculin; see Fig. 6C, and Supplementary Material 3 for *p*-values].

To obtain an overview of the contribution of the tyrosine kinome to melanoma invasion and invadopodia formation, we analyzed the expression patterns of all tyrosine kinases, and their distribution among the 4 clusters (Supplementary Fig. 5). A group of 13 tyrosine kinases were co-expressed with high AXL/low ERRB3 levels (Cluster 2; see Supplementary Material 3); among these, PDGFRA and PDGFRB, EGFR and FGFR1. In contrast, another group of 11 tyrosine kinases negatively co-expressed with high ERRB3/low AXL (Cluster 1; see Supplementary Material 3); among them, two other members of the TAM receptor family, MER and TYRO3, as well as Syk and CSK (Supplementary Fig. 5). Other tyrosine kinases were not

differentially expressed among the clusters. This analysis further supports the notion of two alternative pathways that regulate cell invasion in melanoma.

Discussion

In this study, we describe the molecular cross-talk between different tyrosine kinases involved in the regulation of invadopodia formation and function in melanoma cells. Using a comprehensive siRNA screen, we identified several novel positive invadopodia regulators in A375 metastatic melanoma cells, including TYK2, IGF1R, TYRO3, FES, ALK, ERBB3 and PTK7 (Fig. 1D, 1F; Table 1). In addition, we found 3 kinases (CSK, ABL2 and AXL) whose KD up-regulated invadopodia formation and function (Fig. 1E, 1F; Table 1). A few of these kinases (CSK, ABL2, ERBB3 and PTK7) were reported to regulate invadopodia in other cellular systems (5,13,18,20,36); CSK, for example, is a negative regulator of invadopodia, due to its inhibitory effect on SRC family kinases (SKF) (5,18), which are known to play an essential role in invadopodia formation by phosphorylating and activating key structural components of invadopodia, including TKS5 and cortactin (37).

It is noteworthy that while KD of CSK, which phosphorylates multiple SFKs, elevates invadopodia formation (5), KD of individual SFKs (including Src) had a limited effect on invadopodia formation (Supplementary Material 2). This phenotype may be attributed to the compensatory activity of other SFKs, which are prominently expressed in melanoma tumors (38).

Similarly, functional redundancy between tyrosine kinases that regulate invadopodia, was also implied by marked differences between the profiles of invadopodia modulators in A375 and 63T cells (Fig. 1D, 1E; Supplementary Fig. 1D; Table 1; Supplementary Table 1). Specifically, only

4 genes out of 10 caused similar effects on invadopodia in 63T cells (See Table 1, Supplementary Table 1). These differences may also be attributed to the different driver mutations in the cells, as A375 is a BRAF mutant, while 63T is an NRAS mutant. Clarification of these cellular variations is required for a deeper understanding of invadopodia formation, and for assessing their roles in melanoma metastasis.

In this comprehensive analysis, we found that the RTK AXL acts as a dual-function regulator of invadopodia in both the A375 and 63T melanoma cell lines. AXL is known to be associated with an invasive phenotype in multiple cancers, including melanoma (39). In addition, AXL was shown to be involved in drug resistance mechanisms in melanoma and other cancers (25). Our novel finding that AXL is involved in the regulation of invadopodia formation and function (Fig. 3; Fig. 4) adds another dimension to our understanding of how AXL contributes to the development of these aggressive phenotypes.

The dual role of AXL is manifested by increased invadopodia formation and function upon AXL KD in 4 different melanoma cells lines (A375, 63T, WM793, and A2058) (Fig. 3A-3F; Supplementary Fig. 2G-2I). On the other hand, we demonstrate the positive role of AXL in invadopodia formation and function, based on a series of experiments involving two melanoma cell lines (A375 and 63T). AXL localizes specifically to invadopodia structures at various stages of their formation (Fig. 3G, 3H) and causes an increase in invadopodia activity following overexpression of WT-AXL, but not its kinase-dead mutant (Fig. 4A-4C). Consequently, the capacity of these cells to invade in a Matrigel™ trans-well invasion assay was increased as well (Supplementary Fig. 3B, 3C). Activation of AXL by its ligand, Gas6, increased invadopodia function in both cell lines (Fig. 4D, 4E and Supplementary Fig. 3E), while short-term (6 hr) treatment of cells with the AXL inhibitor R428 was found to block invadopodia function in 4

melanoma cell lines (Figure 4F-4I; Supplementary Fig. 3G, 3H), as well as in 4T1 breast cancer cells (Supplementary Fig. 3G, 3H). Finally, KD of AXL in the metastatic breast cancer cell line MDA-231 caused a significant reduction in invadopodia function (Supplementary Fig. 3I, 3J). Further experiments clarified the dual role of AXL in the regulation of invadopodia. Upon AXL KD or prolonged treatment with the AXL inhibitor (2 days), there was no reduction in AXL phosphorylation on tyrosine Y779 (Fig. 5A, 5B; Supplementary Fig. 4C), although total AXL phosphorylation levels were reduced (Supplementary Fig. 4A, 4B). Under those conditions, both the expression and phosphorylation levels of ERBB3 increased (Fig. 5C, 5G), suggesting a compensatory mechanism for the loss of AXL by ERBB3, potentially leading to an increase in invadopodia function (Fig. 3A, 3B, 5H). This phosphorylation state was accompanied by enhanced phosphorylation of key invadopodia regulators, including SRC, AKT and cortactin (Fig. 5D-5G).

A role for ERBB3 in invadopodia function in melanoma is also supported by the fact that ERBB3 was determined to be one of the invadopodia regulators in the A375 screen described above (Fig. 1D, 1F; Table 1), and by increased invadopodia formation upon treatment of both A375 and 63T cells with the ERBB3 ligand, neuregulin (Fig. 5N, 5O).

Is ERBB3 unique in its capacity to compensate for AXL loss in invadopodia regulation? We cannot exclude the possibility that other tyrosine kinases can compensate for the loss of AXL; yet double KD of both AXL and ERBB3 is sufficient to abrogate the increase in invadopodia formation (Fig. 5L, 5M), and other RTKs did not show dramatic changes in their phosphorylation levels upon AXL KD (Supplementary Fig. 4A, 4B).

Examination of AXL/ERBB3 expression levels in 62 melanoma cell lines included in the *CCLE* database shows significant inverse expression patterns in ~50% of the cells (Fig. 6A, Clusters 1 and 2). Interestingly, ERBB3 levels positively correlate with MITF expression levels, and with three of its main downstream targets (Fig. 6A, Clusters 1 and 2). MITF has been shown to negatively correlate with AXL in melanoma cells (40,41). MITF levels are also known to affect melanoma progression, and fine-tuning of its expression leads to various physiological and pathological manifestations, including cell differentiation, proliferation, apoptosis and invasion (33,41). Furthermore, the balance between MITF and AXL can change cell fate, invasiveness and drug resistance in melanoma (33,41).

The fact that only prolonged inhibition of AXL (~ 2 days), leads to elevated ERBB3 levels (Fig. 5I) and consequently, to increased invadopodia formation (Fig. 5H), suggests that the compensatory mechanism is regulated either at the transcriptional level, or during a slow, post-translational process that affects ERBB3 stability. Notably, similar reciprocal cross-talk between AXL and ERBB3 was reported in breast cancer cells, where prolonged (1-2 days) inhibition of AXL by inhibitor or siRNA treatment led to an elevation in ERBB3 phosphorylation and activity (30).

Note that the CCLE database is based on RNA expression levels in the various cells lines, and demonstrates heterogeneity in the expression patterns of AXL and ERBB3 (Fig. 6A). Our data show an interplay between them mostly on the protein level (Fig. 5C), in cells that express both high AXL and high ERBB3 (A375, Cluster 4). Under AXL perturbation, changes in ERBB3 expression and phosphorylation are seen. Other cells (e.g., those in Clusters 1 and 2) will predominantly express, at steady state, only one of them, at high levels.

One possible mechanism underlying post-transcriptional ERBB3 regulation is an AKT negative feedback loop, mediated through the E3 ligase Nrdp1 and the Nrdp1 regulator USP8, which target ERBB3 to proteasomal degradation (32). USP8 can be phosphorylated and stabilized by AKT, which is activated by ERBB3, thus creating a negative feedback loop for ERBB3 activation (32). In line with that, ERBB3 was shown to display increased membrane localization and activity that compensate for the loss of ERBB family kinases upon tyrosine kinase inhibitor treatment. This compensation was also mediated by AKT negative feedback signaling (42).

Inhibition of the PI3K-AKT pathway can occur upon AXL perturbation (23,43,44). In the absence of AKT there is less ERBB3 ubiquitination for degradation by Nrdp1, a situation that can result in increased ERBB3 protein levels and phosphorylation (32). ERRB3 over-expression and activation, together with activation of another RTK (28,30) can result in increased AXL Y779 phosphorylation, activated PI3K pathway and invadopodia formation (10). Both EGFR and HER2 were shown to directly phosphorylate AXL on Y779 (45,46). Y779 phosphorylation was shown to be one of three auto-phosphorylation sites in the protein c-terminus, and constitute a docking site for a variety of signaling proteins, including PI3K, Grb2, PLCγ, c-src and lck (23), which can lead to enhanced invadopodia formation (4).

To conclude, the findings reported here suggest two possible modes of action for invadopodia regulation in melanoma (Fig. 6D, Proposed Model). One is governed by AXL which is activated by Gas6 (39), and can promote cell invasion and migration, cytoskeletal remodeling (47) and invadopodia formation and function (our results; Fig. 4). This can be achieved by activation of invadopodia-associated proteins (e.g., TKS5 and cortactin) by Src family kinases and the PI3K pathway [(10,48); see also Fig. 6D, Proposed Model]. Indeed, high expression levels of core

invadopodia components such as TKS5, MMP2, ABL1, fascin and vinculin (4) correlate with high AXL levels (Fig. 6C, Cluster 2), as well as an invasive phenotype (Fig. 6A, 6B, Cluster 2).

The second invadopodia-stimulating pathway is induced by ERRB3, which predominantly correlates with a proliferative phenotype (Fig. 6B). Yet upon suppression of AXL, the negative feedback loop mediated by AKT is broken, and ERBB3 is less degraded by its E3 ligase, Nrdp1 (32,49). Under those conditions, ERBB3 protein can be elevated and phosphorylated, and either promote invadopodia function on its own, or mediate residual AXL phosphorylation with another active member of the ERBB family (50), leading to increased invadopodia formation (Fig. 5; Fig. 6D, Proposed Model).

The process of cell invasion includes differential regulation of the migratory and invasive capacities of the cells (2). A finely-tuned balance between the invadopodia regulators AXL and ERBB3 is necessary for the first steps of invasion, that require immediate remodeling of the extracellular matrix. Further cellular dissemination will require the integration of the migratory machinery, which can also be regulated by AXL (24,26).

Our new insights into the unique abilities of AXL and ERBB3 to regulate invadopodia function, together with a deeper understanding of the molecular cross-talk within the kinome network, and their downstream targets in invadopodia, will facilitate the design of an effective combinatorial therapy targeting the metastatic process.

Acknowledgments

We thank Yosef Yarden (Weizmann Institute of Science, Israel) for providing reagents for ERRB3 detection, and scientific advice regarding ERBB3. We thank Aaron Meyer (Massachusetts Institute of Technology, USA) for his generous gift of AXL expression plasmids.

We thank Meenhard Herlyn for his kind gift of WM793 and A2508 cells (Wistar Institute, Philadelphia, PA, USA). We thank the Genomics Center of Biomedical Core Facility (Technion, Israel) for cell authentication tests. We thank Itay Tirosh (Weizmann Institute of Science, Israel), Daniel Peeper and Oscar Krijgsman (Netherlands Cancer Institute, Amsterdam, Netherlands) and Tamar Geiger (Tel-Aviv University, Israel) for insightful discussions and scientific advice regarding AXL/ERBB3 cross-talk in melanoma.

Grants: Israel Ministry of Science (IMOS) French Program Grant no. 3-13024, and an Israel Science Foundation Grant no. 2749/17

Benjamin Geiger is the incumbent of the Erwin Neter Professorial Chair in Cell and Tumor Biology.

References

1. Lideikaitė A, Mozūraitienė J, Letautienė S. Analysis of prognostic factors for melanoma patients. Acta medica Litu. Lithuaniae Academia Scientiarum; 2017;24:25–34. Available from: http://www.ncbi.nlm.nih.gov/pubmed/28630590
2. Friedl P, Wolf K. Tumour-cell invasion and migration: diversity and escape mechanisms. Nat Rev Cancer. 2003;3:362–74. Available from: http://www.ncbi.nlm.nih.gov/pubmed/12724734
3. Nürnberg A, Kitzing T, Grosse R. Nucleating actin for invasion. Nat Rev Cancer. 2011;11:177–87. Available from: http://www.ncbi.nlm.nih.gov/pubmed/21326322
4. Revach O-Y, Geiger B. The interplay between the proteolytic, invasive, and adhesive domains of invadopodia and their roles in cancer invasion. Cell Adh Migr. Taylor & Francis; 2014;8:215–25. Available from: http://www.tandfonline.com/doi/abs/10.4161/cam.27842
5. Murphy DA, Courtneidge SA. The "ins" and "outs" of podosomes and invadopodia: characteristics, formation and function. Nat Rev Mol Cell Biol. NIH Public Access; 2011;12:413–26. Available from: http://www.ncbi.nlm.nih.gov/pubmed/21697900
6. Sibony-Benyamini H, Gil-Henn H. Invadopodia: The leading force. Eur J Cell Biol. 2012;91:896–901. Available from: http://www.ncbi.nlm.nih.gov/pubmed/22633185
7. Buccione R, Caldieri G, Ayala I. Invadopodia: specialized tumor cell structures for the

focal degradation of the extracellular matrix. Cancer Metastasis Rev. 2009;28:137–49. Available from: http://www.ncbi.nlm.nih.gov/pubmed/19153671

8. Yamaguchi H, Condeelis J. Regulation of the actin cytoskeleton in cancer cell migration and invasion. Biochim Biophys Acta - Mol Cell Res. 2007;1773:642–52. Available from: http://www.ncbi.nlm.nih.gov/pubmed/16926057

9. Bromann PA, Korkaya H, Courtneidge SA. The interplay between Src family kinases and receptor tyrosine kinases. Oncogene. 2004;23:7957–68. Available from: http://www.ncbi.nlm.nih.gov/pubmed/15489913

10. Yamaguchi H, Yoshida S, Muroi E, Yoshida N, Kawamura M, Kouchi Z, et al. Phosphoinositide 3-kinase signaling pathway mediated by p110α regulates invadopodia formation. J Cell Biol. 2011;193:1275–88. Available from: http://www.ncbi.nlm.nih.gov/pubmed/21708979

11. Courtneidge SA. Cell migration and invasion in human disease: the Tks adaptor proteins. Biochem Soc Trans. 2012;40:129–32. Available from: http://biochemsoctrans.org/lookup/doi/10.1042/BST20110685

12. Clark ES, Whigham AS, Yarbrough WG, Weaver AM. Cortactin is an essential regulator of matrix metalloproteinase secretion and extracellular matrix degradation in Invadopodia. Cancer Res. 2007;67:4227–35. Available from: http://www.ncbi.nlm.nih.gov/pubmed/17483334

13. Mader CC, Oser M, Magalhaes MAO, Bravo-Cordero JJ, Condeelis J, Koleske AJ, et al. An EGFR-Src-Arg-Cortactin pathway mediates functional maturation of invadopodia and breast cancer cell invasion. Cancer Res. 2011;71:1730–41. Available from: http://www.ncbi.nlm.nih.gov/pubmed/21257711

14. Ikeda K, Wang L-H, Torres R, Zhao H, Olaso E, Eng FJ, et al. Discoidin domain receptor 2 interacts with Src and Shc following its activation by Type I Collagen. J Biol Chem. 2002;277:19206–12. Available from: http://www.ncbi.nlm.nih.gov/pubmed/11884411

15. Knowles LM, Malik G, Pilch J. Plasma fibronectin promotes tumor cell survival and invasion through regulation of Tie2. J Cancer. 2013;4:383–90. Available from: http://www.jcancer.org/v04p0383.htm

16. Revach O-Y, Weiner A, Rechav K, Sabanay I, Livne A, Geiger B. Mechanical interplay between invadopodia and the nucleus in cultured cancer cells. Sci Rep. 2015;5:9466. Available from: http://www.ncbi.nlm.nih.gov/pubmed/25820462

17. Kelley LC, Ammer AG, Hayes KE, Martin KH, Machida K, Jia L, et al. Oncogenic Src requires a wild-type counterpart to regulate invadopodia maturation. J Cell Sci. 2010;123:3923–32. Available from: http://www.ncbi.nlm.nih.gov/pubmed/20980387

18. Okada M. Regulation of the Src Family Kinases by Csk. Int J Biol Sci. 2012;8:1385–97. Available from: http://www.ncbi.nlm.nih.gov/pubmed/23139636

19. Golubkov VS, Prigozhina NL, Zhang Y, Stoletov K, Lewis JD, Schwartz PE, et al.

Protein-tyrosine pseudokinase 7 (PTK7) directs cancer cell motility and metastasis. J Biol Chem. American Society for Biochemistry and Molecular Biology; 2014; 289:24238–49. Available from: http://www.ncbi.nlm.nih.gov/pubmed/25006253

20. Eckert JM, Byer SJ, Clodfelder-Miller BJ, Carroll SL. Neuregulin-1 beta and neuregulin-1 alpha differentially affect the migration and invasion of malignant peripheral nerve sheath tumor cells. Glia. NIH Public Access; 2009;57:1501–20. Available from: http://www.ncbi.nlm.nih.gov/pubmed/19306381

21. Meirson T, Genna A, Lukic N, Makhnii T, Alter J, Sharma VP, et al. Targeting invadopodia-mediated breast cancer metastasis by using ABL kinase inhibitors. Oncotarget. Impact Journals, LLC; 2018;9:22158–83. Available from: http://www.ncbi.nlm.nih.gov/pubmed/29774130

22. Prickett TD, Agrawal NS, Wei X, Yates KE, Lin JC, Wunderlich JR, et al. Analysis of the tyrosine kinome in melanoma reveals recurrent mutations in ERBB4. Nat Genet. 2009;41:1127–32. Available from: http://www.ncbi.nlm.nih.gov/pubmed/19718025

23. Lemke G. Biology of the TAM receptors. Cold Spring Harb Perspect Biol. Cold Spring Harbor Laboratory Press; 2013;5:a009076. Available from: http://www.ncbi.nlm.nih.gov/pubmed/24186067

24. Uribe DJ, Mandell EK, Watson A, Martinez JD, Leighton JA, Ghosh S, et al. The receptor tyrosine kinase AXL promotes migration and invasion in colorectal cancer. Castresana JS, editor. PLoS One. Public Library of Science; 2017;12:e0179979. Available from: http://dx.plos.org/10.1371/journal.pone.0179979

25. Scaltriti M, Elkabets M, Baselga J. Molecular Pathways: AXL, a Membrane Receptor Mediator of Resistance to Therapy. Clin Cancer Res. American Association for Cancer Research; 2016;22:1313–7. Available from: http://www.ncbi.nlm.nih.gov/pubmed/26763248

26. Linger RMA, Keating AK, Earp HS, Graham DK. TAM Receptor Tyrosine Kinases: biologic functions, signaling, and potential therapeutic targeting in human cancer. Adv Cancer Res. 2008. page 35–83. Available from: http://www.ncbi.nlm.nih.gov/pubmed/18620092

27. Liu L, Greger J, Shi H, Liu Y, Greshock J, Annan R, et al. Novel mechanism of Lapatinib resistance in HER2-positive breast tumor cells: activation of AXL. Cancer Res. 2009;69:6871–8. Available from: http://www.ncbi.nlm.nih.gov/pubmed/19671800

28. Vouri M, Croucher DR, Kennedy SP, An Q, Pilkington GJ, Hafizi S. Axl-EGFR receptor tyrosine kinase hetero-interaction provides EGFR with access to pro-invasive signalling in cancer cells. Oncogenesis. Nature Publishing Group; 2016;5:e266. Available from: http://www.nature.com/doifinder/10.1038/oncsis.2016.66

29. Meyer AS, Miller MA, Gertler FB, Lauffenburger DA. The receptor AXL diversifies EGFR signaling and limits the response to EGFR-targeted inhibitors in triple-negative breast cancer cells. Sci Signal. NIH Public Access; 2013;6:ra66. Available from:

http://www.ncbi.nlm.nih.gov/pubmed/23921085

30. Torka R, Pénzes K, Gusenbauer S, Baumann C, Szabadkai I, Őrfi L, et al. Activation of HER3 Interferes with Antitumor Effects of Axl Receptor Tyrosine Kinase Inhibitors: Suggestion of Combination Therapy. Neoplasia. 2014;16:301–18. Available from: http://www.ncbi.nlm.nih.gov/pubmed/24862757

31. Cook RS, Garrett JT, Sánchez V, Stanford JC, Young C, Chakrabarty A, et al. ErbB3 ablation impairs PI3K/Akt-dependent mammary tumorigenesis. Cancer Res. NIH Public Access; 2011;71:3941–51. Available from: http://www.ncbi.nlm.nih.gov/pubmed/21482676

32. Cao Z, Wu X, Yen L, Sweeney C, Carraway KL, III. Neuregulin-induced ErbB3 downregulation is mediated by a protein stability cascade involving the E3 ubiquitin ligase Nrdp1. Mol Cell Biol. American Society for Microbiology (ASM); 2007;27:2180–8. Available from: http://www.ncbi.nlm.nih.gov/pubmed/17210635

33. Müller J, Krijgsman O, Tsoi J, Robert L, Hugo W, Song C, et al. Low MITF/AXL ratio predicts early resistance to multiple targeted drugs in melanoma. Nat Commun. NIH Public Access; 2014;5:5712. Available from: http://www.ncbi.nlm.nih.gov/pubmed/25502142

34. Dugo M, Nicolini G, Tragni G, Bersani I, Tomassetti A, Colonna V, et al. A melanoma subtype with intrinsic resistance to BRAF inhibition identified by receptor tyrosine kinases gene-driven classification. Oncotarget. Impact Journals, LLC; 2015;6:5118–33. Available from: http://www.ncbi.nlm.nih.gov/pubmed/25742786

35. Widmer DS, Cheng PF, Eichhoff OM, Belloni BC, Zipser MC, Schlegel NC, et al. Systematic classification of melanoma cells by phenotype-specific gene expression mapping. Pigment Cell Melanoma Res. 2012;25:343–53. Available from: http://www.ncbi.nlm.nih.gov/pubmed/22336146

36. Peradziryi H, Tolwinski NS, Borchers A. The many roles of PTK7: A versatile regulator of cell–cell communication. Arch Biochem Biophys. 2012; 524:71–6. Available from: http://www.ncbi.nlm.nih.gov/pubmed/22230326

37. Tehrani S, Tomasevic N, Weed S, Sakowicz R, Cooper JA. Src phosphorylation of cortactin enhances actin assembly. Proc Natl Acad Sci U S A. National Academy of Sciences; 2007;104:11933–8. Available from: http://www.ncbi.nlm.nih.gov/pubmed/17606906

38. Buettner R, Mesa T, Vultur A, Lee F, Jove R. Inhibition of src family kinases with Dasatinib blocks migration and invasion of human melanoma cells. Mol Cancer Res. 2008;6:1766–74. Available from: http://www.ncbi.nlm.nih.gov/pubmed/19010823

39. Lemke G. Biology of the TAM receptors. Cold Spring Harb Perspect Biol. Cold Spring Harbor Laboratory Press; 2013;5:a009076. Available from: http://www.ncbi.nlm.nih.gov/pubmed/24186067

40. Müller J, Krijgsman O, Tsoi J, Robert L, Hugo W, Song C, et al. Low MITF/AXL ratio predicts early resistance to multiple targeted drugs in melanoma. Nat Commun. 2014;5:5712. Available from: http://www.ncbi.nlm.nih.gov/pubmed/25502142

41. Tirosh I, Izar B, Prakadan SM, Wadsworth MH, Treacy D, Trombetta JJ, et al. Dissecting the multicellular ecosystem of metastatic melanoma by single-cell RNA-seq. Science. NIH Public Access; 2016;352:189–96. Available from: http://www.ncbi.nlm.nih.gov/pubmed/27124452

42. Sergina N V, Rausch M, Wang D, Blair J, Hann B, Shokat KM, et al. Escape from HER-family tyrosine kinase inhibitor therapy by the kinase-inactive HER3. Nature. NIH Public; 2007;445:437–41. Available from: http://www.ncbi.nlm.nih.gov/pubmed/17206155

43. Zuo Q, Liu J, Huang L, Qin Y, Hawley T, Seo C, et al. AXL/AKT axis mediated-resistance to BRAF inhibitor depends on PTEN status in melanoma. Oncogene. Nature Publishing Group; 2018;37:3275–89. Available from: http://www.nature.com/articles/s41388-018-0205-4

44. Holland SJ, Pan A, Franci C, Hu Y, Chang B, Li W, et al. R428, a Selective Small Molecule Inhibitor of Axl Kinase, Blocks Tumor Spread and Prolongs Survival in Models of Metastatic Breast Cancer. Cancer Res. 2010; 70:1544–54. Available from: http://www.ncbi.nlm.nih.gov/pubmed/20145120

45. Vouri M, Croucher DR, Kennedy SP, An Q, Pilkington GJ, Hafizi S. Axl-EGFR receptor tyrosine kinase hetero-interaction provides EGFR with access to pro-invasive signalling in cancer cells. Oncogenesis; 2016;5:e266. Available from: http://www.ncbi.nlm.nih.gov/pubmed/27775700

46. Goyette M-A, Duhamel S, Aubert L, Pelletier A, Savage P, Thibault M-P, et al. The Receptor Tyrosine Kinase AXL Is Required at Multiple Steps of the Metastatic Cascade during HER2-Positive Breast Cancer Progression. Cell Rep. Cell Press; 2018;23:1476–90. Available from: https://www.sciencedirect.com/science/article/pii/S2211124718305485?via%3Dihub

47. Paccez JD, Vogelsang M, Parker MI, Zerbini LF. The receptor tyrosine kinase Axl in cancer: Biological functions and therapeutic implications; Available from: https://onlinelibrary.wiley.com/doi/pdf/10.1002/ijc.28246

48. Coirtneidge S.A, Azuvena E.F., Pass, I., Seals, D.F., Tesfay L. The Src Substrate Tks5, Podosomes (Invadopodia), and Cancer Cell Invasion. Cold Spring Harb Symp Quant Biol. 2005;70:167–71. Available from: http://www.ncbi.nlm.nih.gov/pubmed/16869750

49. Campbell MR, Amin D, Moasser MM. HER3 comes of age: new insights into its functions and role in signaling, tumor biology, and cancer therapy. Clin Cancer Res. NIH Public Access; 2010;16:1373–83. Available from: http://www.ncbi.nlm.nih.gov/pubmed/20179223

50. Yarden Y. The EGFR family and its ligands in human cancer. signalling mechanisms and therapeutic opportunities. Eur J Cancer. 2001;37 Suppl 4:S3-8. Available from:

http://www.ncbi.nlm.nih.gov/pubmed/11597398

Tables

Gene knock-down	Degradation/cell (normalized)	*p*-value	Phenotype
TYK2	0.19	4.03E-04	less invadopodia
IGF1R	0.38	9.24E-05	less invadopodia
TYRO3	0.21	1.54E-03	less invadopodia
FES	0.17	4.59E-03	less invadopodia
ALK	0.26	3.88E-11	non-mature invadopodia
ERBB3	0.32	9.79E-05	less structures, less TKS5
PTK7	0.34	1.92E-03	less invadopodia
Control	1.00		
ABL2	2.27	2.31E-10	more invadopodia
AXL	2.84	5.60E-03	more invadopodia
CSK	8.31	6.77E-03	more invadopodia

Table 1: Invadopodia regulators in A375 cells.

Normalized degradation/cell is presented for each gene KD in A375 cells.

P-value for each gene is presented. Three repeats; n> 100 for each sample. The phenotype caused by KD of each of the genes, visualized by actin and TKS5 staining and evaluated in a qualitative fashion, is described under the Phenotype heading.

Figures and Figure Legends

Figure 1: Microscopy-based siRNA screen for tyrosine kinases invadopodia regulators in A375 cells.

(A) A375 cells were cultured on gelatin gel for 3 h and stained for phosphorylated tyrosine and actin. White arrows denote invadopodia structures. Scale bar: 20 μm. (B) Representative images from the siCON versus siTOX samples of the screen, used to evaluate transfection efficiency in A375. (C) Real-time analysis of Src gene expression following transfection under screening

conditions in A375; n=3. (D, E) Quantification of normalized degradation/cell for the final list of genes of the screen (invadopodia assay) in A375 cells. D shows genes that caused a reduction in invadopodia function upon KD, and E shows genes that caused an elevation of invadopodia function upon KD. Three repeats; n>100 in each sample. (F) Representative images of A375 cells from the screen. Cells were cultured for 6 h on fluorescently labeled gelatin, and stained with DAPI. Scale bar: 20 μm.

Figure 2: Microscopy-based siRNA screen for tyrosine kinases invadopodia regulators in 63T cells.

(A) 63T cells cultured for 3 h on fluorescently labeled gelatin and stained for actin, show that they degrade the matrix (right image), and form actin dots (left image; invadopodia structures are denoted by white arrows). Scale bar: 10 μm. (B) Representative images from the siCON versus siTOX samples of the screen, used to evaluate transfection efficiency in 63T cells. (C) Real-time analysis of Src gene expression following transfection under screening conditions in 63T cells; n=3. (D) Representative images of 63T cells from the screen. Cells were cultured for 6 h on fluorescently labeled gelatin, and stained with DAPI. Scale bar: 20 μm.

Figure 3: **AXL is localized to invadopodia, and regulates their function.**

(A, B) Invadopodia assay of siCON versus siAXL in A375 and 63T cells, respectively. Cells were cultured for 6 h. Ten repeats for each cell; n>100 in each sample. (C) Representative image of A375 siCON and siAXL cells. Scale bar: 20 μm. (D) Western blot analysis of AXL protein in A375 and 63T cells upon AXL KD. GAPDH was used as a loading control. (E, F) Quantification of invadopodia-forming cells (expressed as a percentage) in A375 and 63T cells, respectively.

Cells were cultured on gelatin gel for 6 h. Three repeats; n>100 in each sample. (G, H) A375 (G) or 63T cells (H) were cultured on fluorescently labeled gelatin for 1.5 h, 3 h, and 6 h, and stained for actin and phosphorylated AXL. AXL localized to invadopodia cores from the early stages of their formation (1.5 h), through the mature stage (6 h). AXL also localized to focal adhesions. Invadopodia structures are denoted by white arrows. Scale bar: 20 μm.

Figure 4: AXL is a positive regulator of invadopodia in melanoma cells.

Invadopodia assay of A375 cells (A, B) or 63T cells (C) overexpressing AXL-WT, AXL kinase-dead (DK), or control plasmid, cultured on fluorescently labeled gelatin for 6 h, and stained for DAPI. Representative images in A; quantification in B and C. Three repeats for each cell type; n>100 in each sample. Scale bar: 20 μm. (D, E) Invadopodia assay of control or 200 ng/ml Gas6-treated cells cultured on fluorescently labeled gelatin for 6 h. Gas6 effective concentrations were varied between experiments, and ranged between 200-1000 ng/ml. Four repeats, n>100 in each sample. Scale bar: 20 μm. (F, G) Invadopodia assay of A375 cultured on fluorescently labeled gelatin for 6 h with DMSO or the AXL inhibitor R428 (in concentrations of 5 μM, 2 μM, or 1 μM). Three repeats for each cell type; n>100. Cells are stained for actin. Scale bar: 20 μm. (H, I) Invadopodia assay of 63T cultured on fluorescently labeled gelatin for 6 h with DMSO or the AXL inhibitor R428 (in concentrations of 5 μM, 2 μM, or 1 μM). Three repeats for each cell type; n>100. Cells are stained for actin. Scale bar: 20 μm.

Figure 5: The ERBB3 pathway is activated when AXL is inhibited for prolonged periods.

(A) Western blot of A375 cells showing AXL phosphorylation (Y779) and total AXL levels of control (siCON), AXL KD (siAXL) or AXL KD with R428 AXL inhibitor treatment (siA+R).

Tubulin served as loading control. Quantifications in (B); n=3. (C) Western blot of A375 cells, showing ERBB3 phosphorylation (Y1289) and total ERBB3 protein in siAXL versus siCON cells. AXL levels are presented. GAPDH served as a loading control. Quantification in (G); n=4. (D, E, F) Western blot of A375 cells, showing Src phosphorylation (Y416) and total Src, cortactin phosphorylation (Y421) and total cortactin and AKT (S437) phosphorylation, and total AKT protein levels in siAXL versus siCON cells, respectively. Quantification in (G), n=3 or more for each protein. (G) Quantifications of Western blots in (C-F). pSRC/SRC graph is truncated due to a wide range of differences in phosphorylation elevation between the phosphoproteins (H). Western blot of A375 cells, showing ERBB3 phosphorylation (Y1289) and total protein in DMSO (D) versus R428 short-term treatment (1μM for 6 h) and DMSO (D-2d) versus R428-2d prolonged treatment (1 μM for 2 days). GAPDH served as a loading control. Quantifications in J; n=3. (I) Western blot of A375 cells, showing cortactin phosphorylation (Y421) and total protein in DMSO (D) versus R428 short-term treatment (1 μM for 6 h) and DMSO (D-2d) versus R428-2d prolonged treatment (1 μM for 2 days). Quantifications in J; n=3. (K) Invadopodia assay of A375 cells incubated for 2 days with 1 μM R428, AXL inhibitor, or DMSO. After 48 h, cells were replated on fluorescently labeled gelatin for 6 h for the invadopodia assay. Invadopodia are denoted by white arrows. Four repeats; n>100 in each sample. (L, M) Invadopodia assay of A375 cells with KD of AXL, ERBB3, AXL+ERBB3 or siCON cultured on fluorescently labeled gelatin for 6 h. Six repeats; n>100 in each sample. (N, O) Invadopodia assay of A375 or 63T cells (two repeats or three repeats, respectively; n>100 in each sample) cultured on fluorescently labeled gelatin for 6 h with 100 ng/ml neuregulin, or vehicle.

Figure 6: AXL negatively correlates with ERBB3 in 50% of melanomas.

(A) Hierarchical clustering by Euclidian distance was applied to the Z-score values of AXL, ERBB3, MITF, and three MITF targets: PMEL, TYRP1, and MELANA, from 62 melanoma cell lines of the *CCLE* Cell Line dataset. Four clusters were selected manually. AXL and ERBB3 are significantly negatively correlated (for *p*-values, see Supplementary Material 3). (B) Prediction of cell phenotype based on the MPSE (Melanoma Phenotype-Specific Expression) signature (34,35). (C) Analysis of Z-score values of 14 core invadopodia proteins among the four clusters described in A. *P*-values for the differences of the proteins in Clusters 1 and 2 are presented in Supplementary Material 3. (D) Proposed model for AXL-ERBB3 interplay in invadopodia regulation. AXL and ERBB3 can both positively regulate invadopodia, depending on their initial balance in the cell. Each of them is activated by its ligand (AXL by Gas6; ERBB3 by neuregulin). A one-directional interplay exists between the two receptors. Once AXL is subjected to short-term inhibition (6 h) by the inhibitor, invadopodia function is inhibited; while AXL is subjected to prolonged inhibition (2 days) by siRNA or inhibitor treatment, ERBB3 can be activated, by destabilization of its E3 ligase complex mediated by an AKT negative feedback loop (See Discussion). The elevation in ERBB3 expression and phosphorylation can activate invadopodia function directly by activation of PI3K, or mediate the phosphorylation of AXL on Y779 together with another RTK, and lead to invadopodia formation. Both AXL and ERBB3 can activate PI3K and SFK, leading to phosphorylation of TKS5 and cortactin, that integrate into the invadopodia core, and initiate their formation. Further actin polymerization and actin bundling by fascin occurs, eventually resulting in the secretion of MMPs, and matrix remodeling.

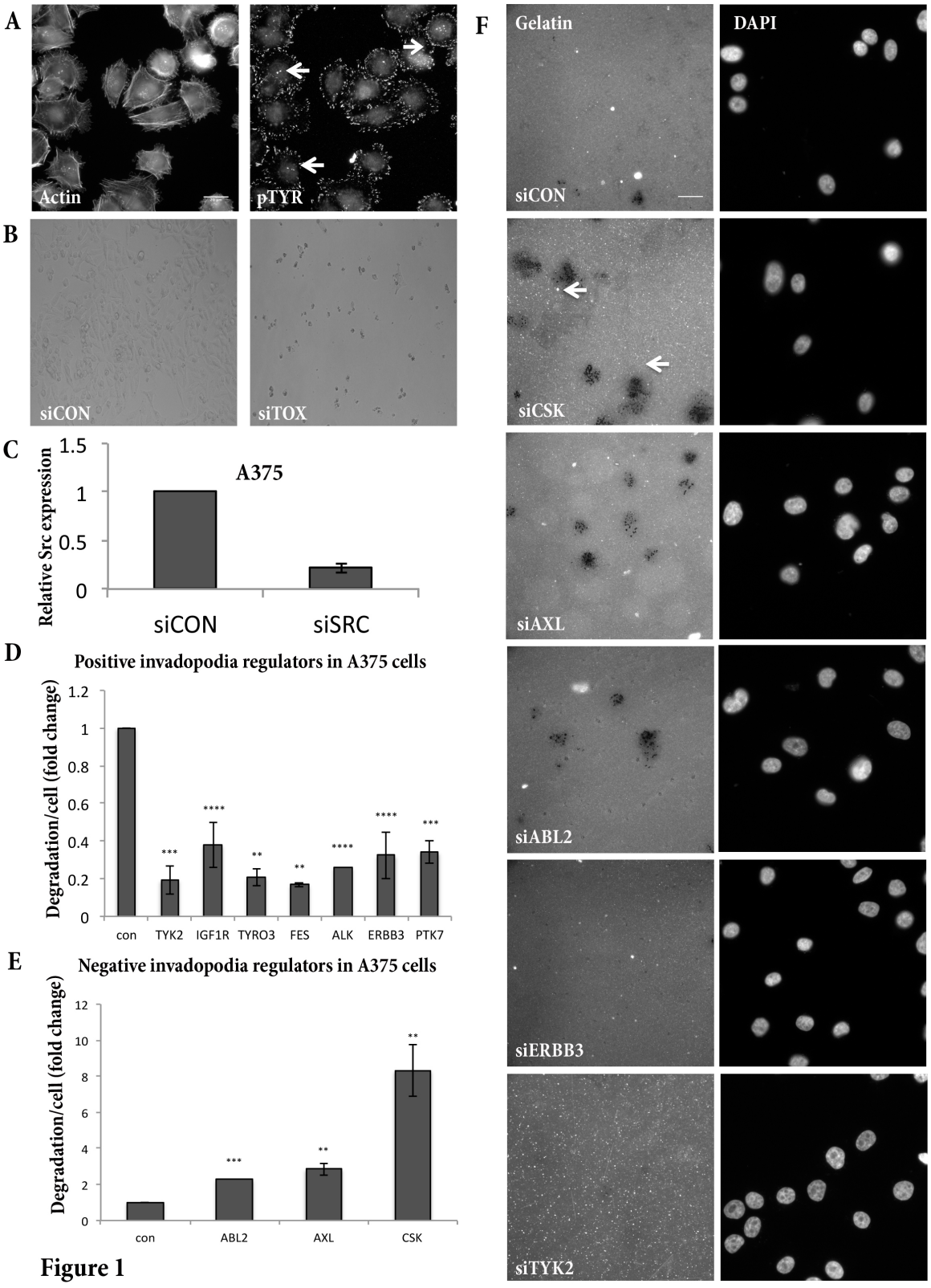

Figure 1

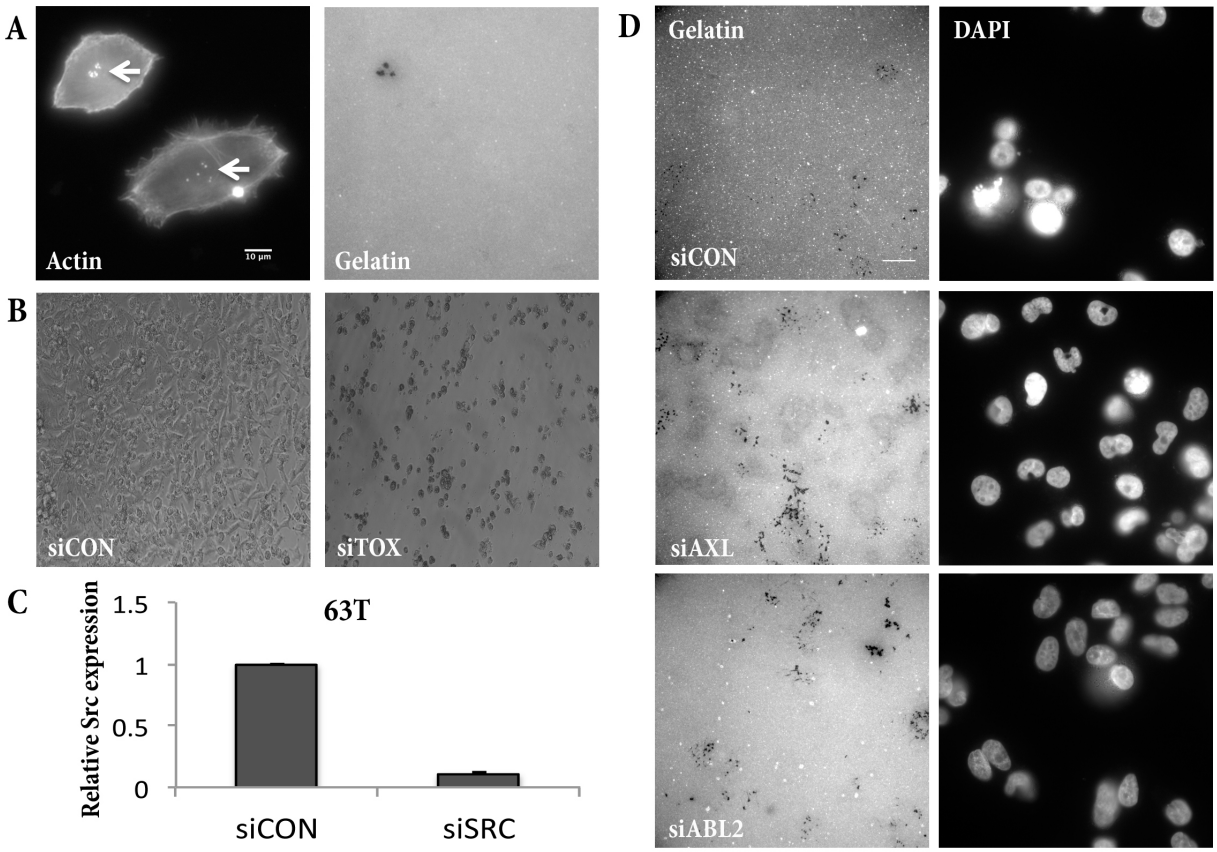

Figure 2

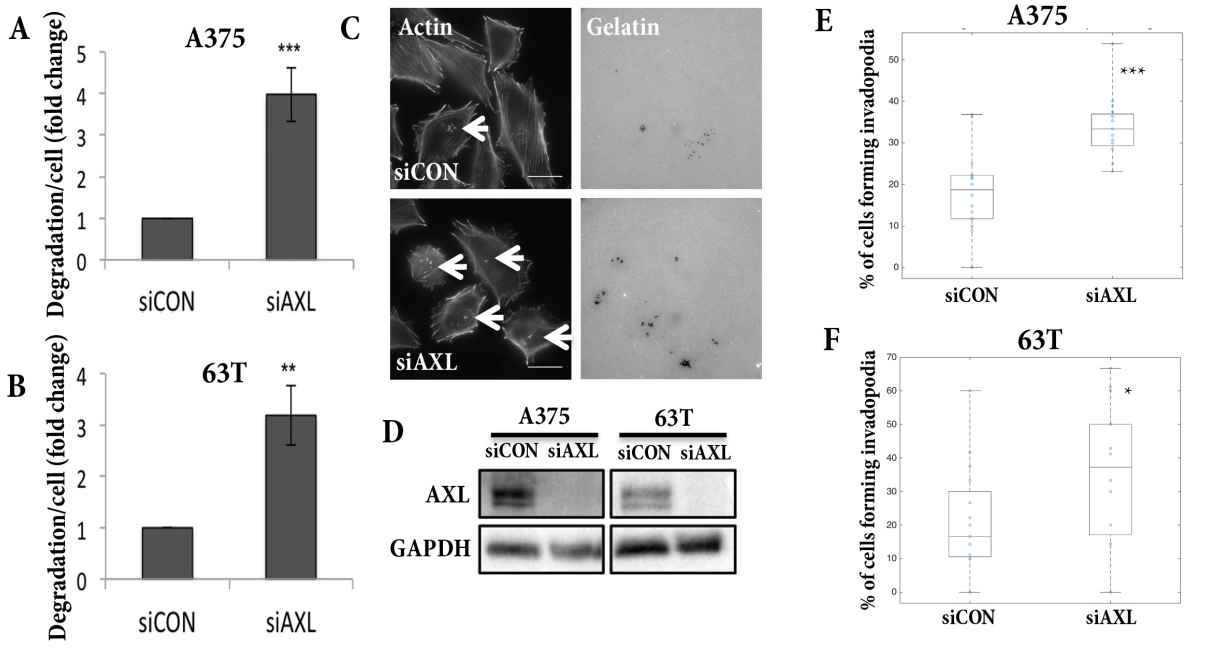

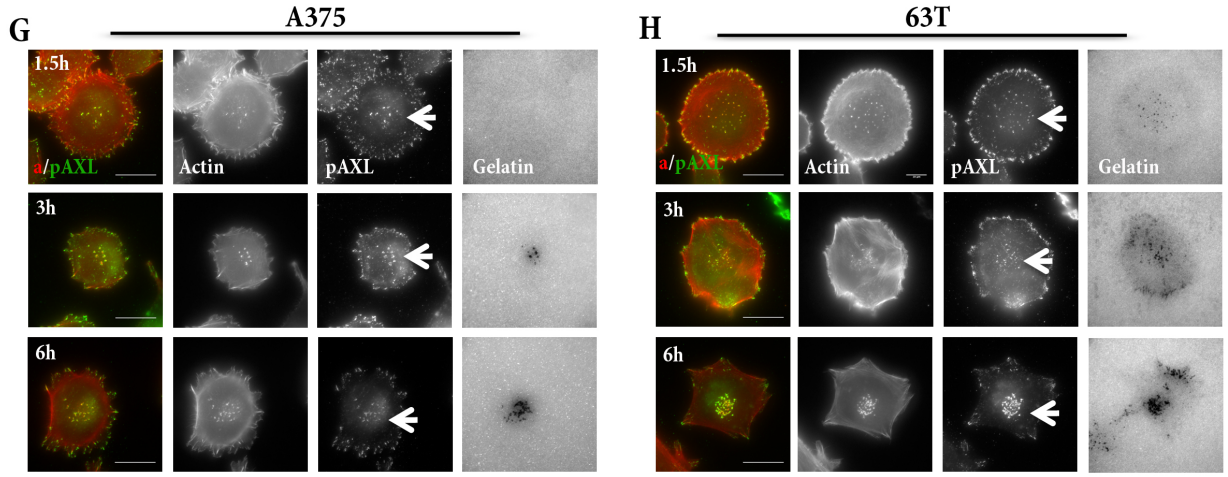

Figure 3

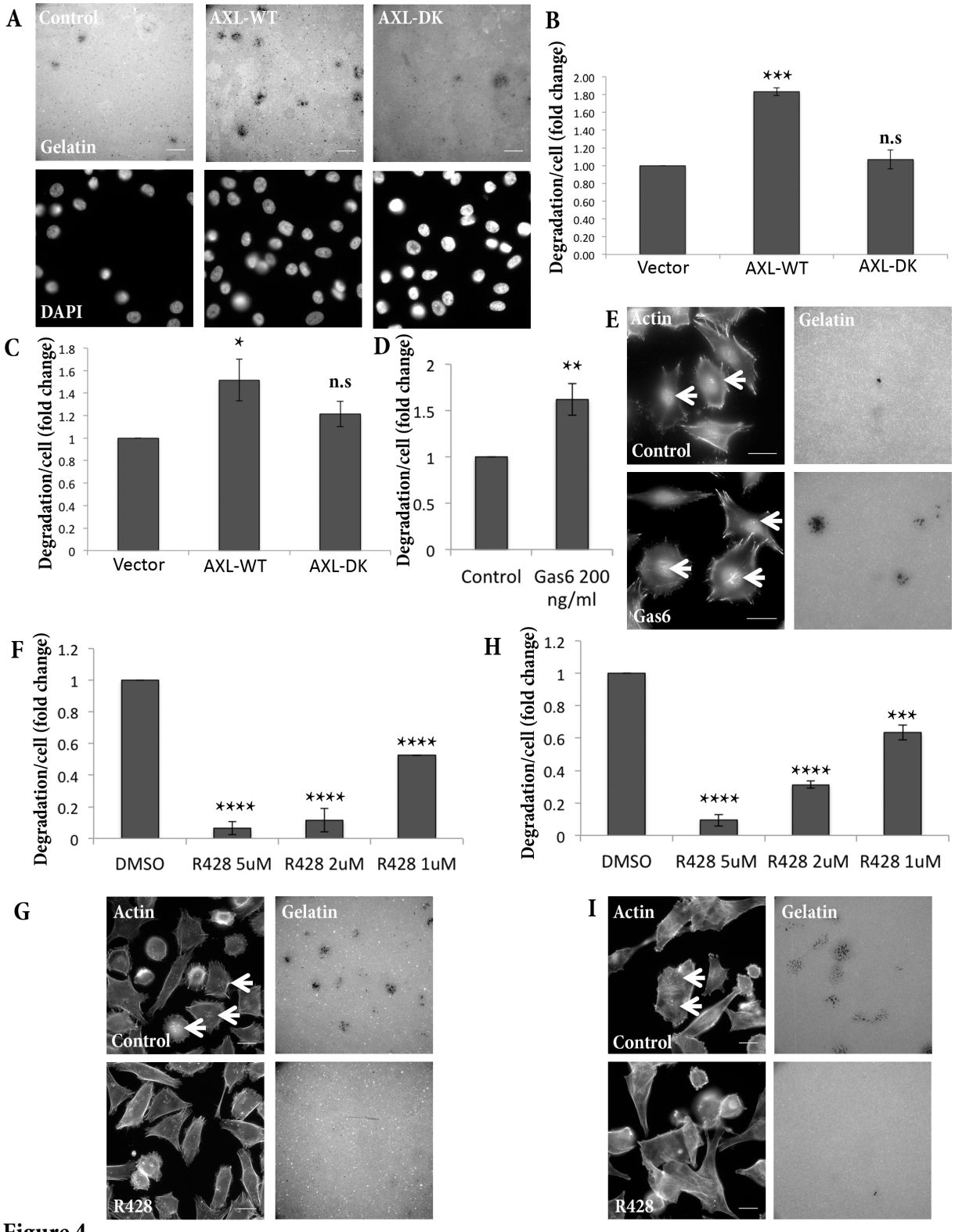

Figure 4

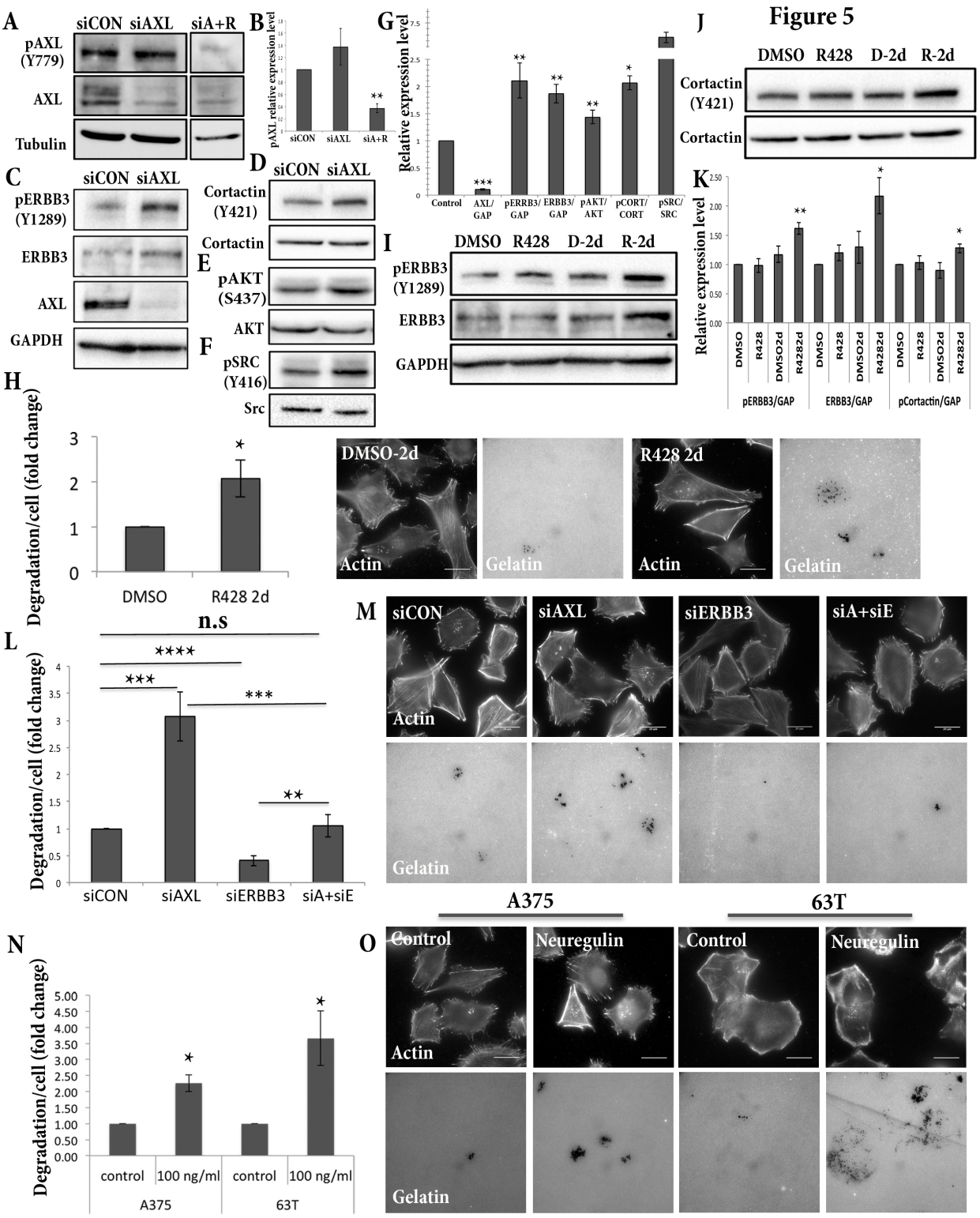

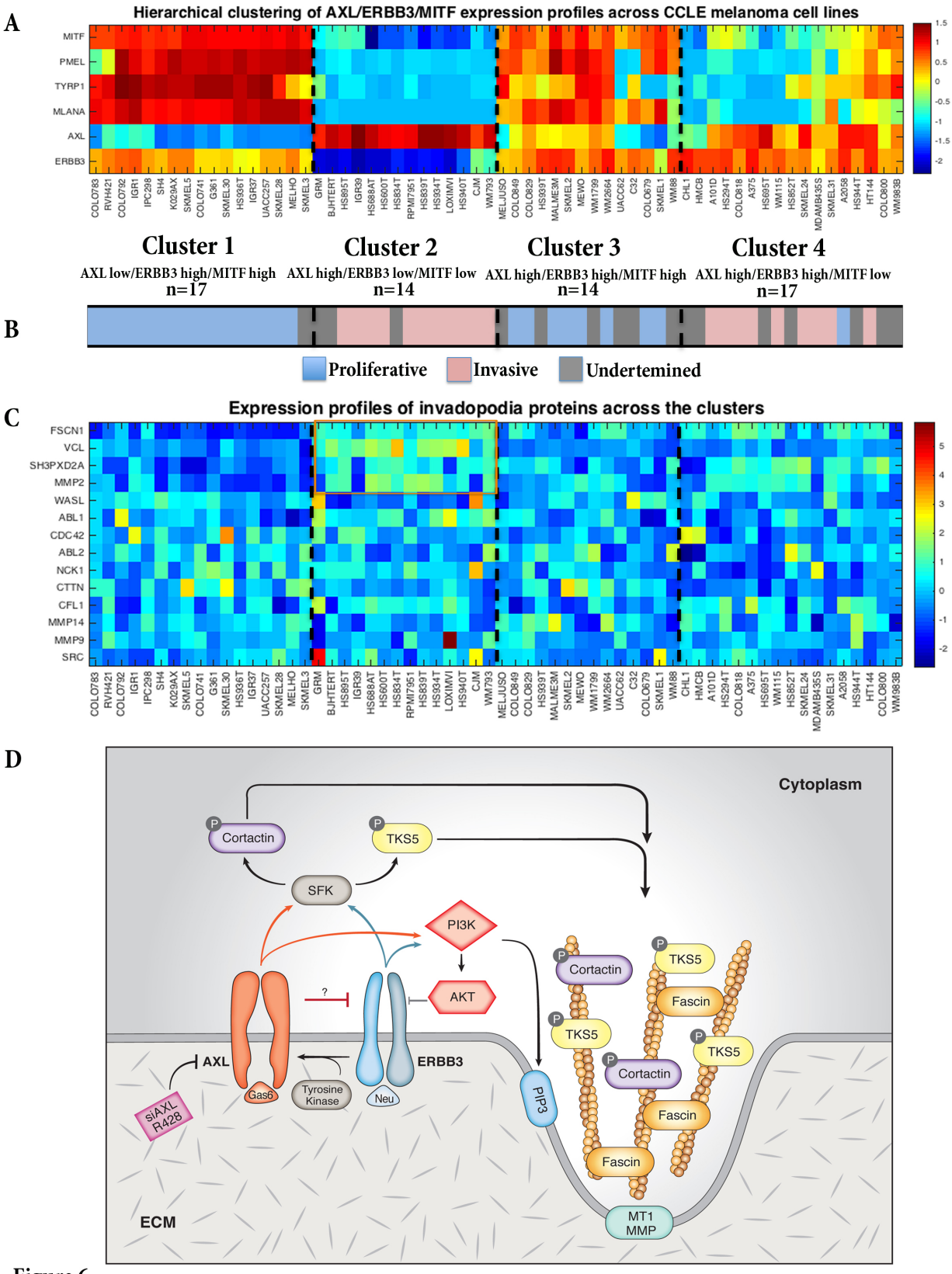

Figure 6